UBMDP: Urban Building Mesh Decoupling and Polygonization

Li Yan, *Member, IEEE*, Yao Li, Jicheng Dai, and Hong Xie

***Abstract*— With the development of photogrammetry, digital city, and metaverse, the 3-D representation of urban buildings has attracted more and more attention. As the main form of the 3-D urban building model, the triangular mesh model has deficiencies such as high complexity, high-data volume, and low-structural information, which seriously restrict its application in spatial analysis and urban planning. This article proposes a hybrid modeling strategy geared toward the mesh model generated from oblique images to obtain building models that are compact, manifold, watertight, and have certain structural and semantic information. First of all, when the planar region topology graph has been established, a topology decoupling strategy is designed to obtain a set of relatively independent topology subgraphs which form a hierarchical structure. After that, to improve model quality, topology optimization of parallel planes has also been studied systematically. Then, we adopt a divide-and-conquer strategy to perform data-driven and model-driven building modeling for the primary and ancillary structures. Finally, a component-level simple polygon model combination is generated. Experiments prove that the proposed method has excellent visual authenticity, structural completeness advantages, and decent LoD3 ability. As a mesh simplification method, the data is compressed to 0.11%–0.75% in a Hausdorff metric around 0.3 m, which further proves that this method is state-of-the-art.**

***Index Terms*— 3-D modeling, building reconstruction, mesh simplification, polygonization, topology decoupling, topology optimization.**

I. Introduction

IN THE field of 3-D geographic information, the concise and high-quality representation of urban building spatial structure information is a far-reaching goal pursued diligently [1], [2], [3], [4]. As the principal places of human activities, urban buildings usually have tall and complex structures and a congested measurement environment. To collect 3-D spatial information on the building surface, laser scanning, and oblique photogrammetry have become the leading technical means. Compared with laser scanning technology, unmanned aerial vehicle (UAV) oblique photogrammetry has received more attention for its flexibility, efficiency, and texture authenticity [5].

The generation of the urban building mesh model has a mature production process using UAV oblique photogrammetry technology. Much open-source software (such as AliceVision and OpenMVS [6], [7], [8]) and commercial software (Agisoft Metashape, ContextCapture, and GodWork [9], [10], [11]) can obtain buildings surface dense mesh models directly. An alternative approach is to use the meshing algorithm (Delaunay triangulation, Poisson reconstruction, and marching cubes [12], [13], [14]) to process the point cloud obtained from the above software. Using dense triangular faces to fit the surface morphology of buildings is a normalized feature of current 3-D urban model applications. The triangulated form has high geometric fitting accuracy, especially after texture mapping, and has a more realistic perception. However, the surge in demand for autonomous driving, intelligent urban management, and metaverse, frequent, and complex spatial analysis has led to an exponential increase in the amount of computation with the number of model surfels [15], [16], [17]. Dense triangular meshes cannot adapt to high-volume model interactions, especially in the face of physical simulation application scenarios, which place excessive demands on computing power.

Building monomerization can facilitate attribute editing, application management, and asynchronous analysis, which has attracted the attention of many researchers [18], [19], [20] yet is not our focus. Some individual buildings are huge complex buildings, such as shopping malls and large office buildings. Given the design paradigm of architectures and the development of the demand for model interaction and analysis, it is necessary and feasible to decompose and simplify the building model furtherly. An independent building consists of a complex roof surface and relatively simple façades to form its primary structure, usually divided into several physically closely connected building blocks for typical urban scenes. The main structure is attached to trivial structures distributed in islands or peninsulas, such as balconies, dormers, hanging air conditioners, and chimneys. Each building block is composed of a small number of simple polygons to form a simple polyhedral solid of a watertight manifold. These polygons also exhibit very significant geometric properties: parallelism, verticality, and horizontality, which together with the adjacency relationship constitute the topological properties of the building.

Manuscript received 2 August 2022; revised 9 November 2022 and 2 March 2023; accepted 10 June 2023. Date of publication 22 June 2023; date of current version 3 July 2023. This work was supported in part by the National Key Research and Development Project of China under Grant 2020YFD1100200, in part by the Open Fund of Hubei Luojia Laboratory under Grant 220100053, and in part by the Science and Technology Major Project of Hubei Province under Grant 2021AAA010. *(Li Yan and Yao Li contributed equally to this work.) (Corresponding author: Hong Xie.)*

Li Yan, Yao Li, and Jicheng Dai are with the School of Geodesy and Geomatics, Wuhan University, Wuhan 430079, China (e-mail: lyan@sgg.whu.edu.cn; whu_liyao@whu.edu.cn; daijicheng@whu.edu.cn).

Hong Xie is with the School of Geodesy and Geomatics, Wuhan University, Wuhan 430079, China, and also with the Hubei Luojia Laboratory, Wuhan 430079, China (e-mail: hxie@sgg.whu.edu.cn).

Digital Object Identifier 10.1109/TGRS.2023.3288590

This work is licensed under a Creative Commons Attribution 4.0 License. For more information, see https://creativecommons.org/licenses/by/4.0/

With a view to these characteristics of urban buildings, this article designs a new framework to generate polygonal models by topology decoupling, topology optimization, and hybrid-driven modeling of building surface triangular mesh models. Under the condition that the input data is a single-building mesh model, we require that our method does not need go through complex parameter adjustment or manual interaction, even for data containing extensive nonbuilding regions or significant noise. In addition, it is efficient to obtain structurally informative, manifold, and watertight polyhedron models or model combinations. The obtained model should be a simple polyhedron model composed of simple polygons. Therefore, we can also call the reconstruction to result in a polygon model. The modeling process is a polyhedronization process and also a polygonization process. Except for not representing the window structure well, the polygon model should have a LoD3 level of representation capability according to the CityGML standard [21].

Our previous work [22] achieved the efficient generation of polyhedral models and improved detailed preservation capabilities by constructing the 1-ring patch and optimizing the parapet structure. For the convenience of expression, we call it UBMP-PaTo in this article. This article goes a step further on this basis. Inheriting the basic flow of 1-ring patch aggregation, plane primitive extraction, topology optimization, and polyhedron model generation, this article adds topology decoupling as a key link after plane primitive extraction. On the premise of topology decoupling, we systematically enrich the content of topology optimization according to the different spatial relationships of parallel planes. Based on the merging of approximately coplanar parallel plane regions and the topology enhancement of inverse parallel planes, this work adds the topology enhancement of stepped parallel planes and the angle adjustment of continuous parallel planes. In the polyhedral model generation phase, we instead use a divide-and-conquer hybrid modeling strategy. The main building block obtained by topology decoupling uses the same modeling strategy as UBMP-PaTo, while the ancillary structures use the topology completion base as a soft constraint. In addition, this article is different from UBMP-PaTo in terms of regional growth and candidate screening rules. Through these improvements, we try to preserve more abundant structural information of the polyhedron model.

Our work has four main contributions to the current state-of-the-art as follows.

1) A hybrid-driven reconstruction framework is designed to realize building mesh polygonization and solid decomposition. Both bottom-up and top-down reconstruction strategies are used in a divide-and-conquer manner.
2) A new methodology of topology decoupling is proposed. According to the spatial and topological relationship, the building plane region is divided into blocks, islands, and peninsula structures.
3) Furthermore, enriches the connotation of topology optimization, especially the optimization of stepped parallel planes, which dramatically improves the fidelity of polygon models.
4) A topological completion library is established to restore ancillary structures with critical topological defects.

II. Related Works

The research on 3-D building reconstruction has a broad connotation, and many of them have inspired us or become the basis of our work. We briefly introduce these related researches. The data sources for 3-D modeling of urban buildings mainly include the image, point cloud, and mesh model [1], [23], [24]. Depending on data sources, 3-D modeling strategies can be divided into model-driven, data-driven, and hybrid-driven [25].

Model-driven or parametric 3-D modeling adopts a top-down approach, using a library of preestablished building model primitives to match the input data and obtain the best model or model combination by primitive selection. Since the model-driven method was proposed at the end of the last century [26], much research has been devoted to improving the primitive library and the primitive selection strategy. Lafarge et al. [27] designed a selection strategy based on the Reversible Jump Markov Chain Monte Carlo Sampler and simulated annealing algorithm for the DSM model. Xiong et al. [28] selected the model structure by searching for the minor cycle of the topology graph. Li and Shan [29] used RANSAC to segment the primitives, used holistic primitive fitting to select the model type, and subsequently used the 3-D bool operation to complete the multiprimitive reconstruction. Such methods can largely make up for the shortcomings of data quality. However, the shapes of buildings are varied, and it is difficult to express all forms with a set of primitive libraries. At the same time, the bloated primitive library will also lead to a sharp drop in primitive search efficiency.

Data-driven or nonparametric modeling has been the most mainstream 3-D modeling strategy in the past two decades. The data-driven strategy has two main characteristics. On the one hand, structural point, structural line, or face information are extracted directly from the original data in a bottom-up manner without relying too much on prior knowledge. Another one is the direct combination into a 3-D model according to the adjacency relationship or spatial intersection relationship. Rottensteiner and Brese [30] proposed a curvature-based roof plane extraction strategy and combined it into a polyhedron model. Wen et al. [31] extracted planar features from airborne and ground point cloud data, extracted line features from stereo images, constructed a region adjacency map using the extracted features as mutual constraints, and finally generated a LoD3 model. Han et al. [19] proposed a vectorized modeling strategy. The photogrammetric mesh finally generates a single LoD2 model after three steps of roof contour extraction, MRF optimization, and roof plane extrusion. Reconstructing buildings using data-driven methods is not limited by the predefined primitive library, and the building forms are more diversified. Still, its dependence on data quality leads to modeling results with a faithful reflection of quality problems or even unpredictable errors.

Applying the hypothesis-and-selection strategy in data-driven modeling has become an attractive research topic.

Sohn et al. [32] used implicit shape rules to generate hypothetical models of roof surfaces from airborne point cloud data. Then gradient descent was used to select polyline models that maximize orthogonality, symmetry, and directional simplicity. Li et al. [33] divided the point cloud data into several candidate cuboids aligned with the coordinate axes under the Manhattan assumption and selected the best subset. PolyFit, proposed by Nan and Wonka [34], transforms the piecewise plane model reconstruction into the binary linear programming selection of candidate planes extracted from point clouds, resulting in manifold, watertight, lightweight polygon models. Liu et al. [35] recovered topological information for incomplete patch primitives based on line-plane relationships. They generated a complete set of candidate planes for the target building, reducing the data-driven approach's dependence on data quality. Bauchet and Lafarge [36] designed a kinetic data structure to partition space into finite convex polyhedra, and a watertight lightweight model was obtained by min-cut optimization. Based on PolyFit, Xie et al. [37] used topology and spatial prior knowledge to reduce the number of candidates' faces to improve reconstruction efficiency. First, enriching candidate edges or candidate's faces and then using mathematical optimization formulas for model generation, this strategy can overcome particular noise and data missing defects. Nevertheless, for input data with distinct signal-to-noise ratios, the quality of the obtained model depends on parameter adjustment, and the optimization of a delicate building model often takes a considerable amount of time.

The simplification from dense building surface meshes to compact models is one way of data-driven modeling. Traditional mesh simplification methods, called mesh decimation, obtain more lightweight model data by removing mesh elements, such as QEM, VSA, and SAMD [38], [39], [40], [41], [42]. These methods starting from local optimization can obtain a simplified model closest to the original mesh model according to the specified compression level. Still, obtaining a building model with a maximum compression of useful information isn't easy. On the premise of piecewise planar, polygonization strategies to extract planes from mesh models and build closed polygonal models have also been developed recently [43], [44]. Bouzas et al. [45] extracted candidate faces and edges from the building mesh model and obtained the optimization results through a binary linear programming equation. This method is referred as SABMP in the later comparison. Our previous work, UBMP-PaTo, greatly improved the efficiency of SABMP, alleviated its reliance on parameter tuning, and complemented the parapet topology, resulting in improved model quality. These global hypothesis-and-selection strategies can overcome some data defects and noise. With appropriate parameter settings, a globally optimal simplified model can be obtained, yet the ability to preserve local structures with important semantic information is still to be improved.

The **hybrid-driven** method tries to overcome the respective drawbacks of the above two ways so that the model can conform to the morphological characteristics of the original data to the greatest extent and make full use of the prior knowledge of architecture. Approaches that claim to be hybrid-driven commonly use a data-driven strategy to detect features first and then use a model-driven strategy to fit prior knowledge or primitives library. According to predefined rules, Tian et al. [46] used ground image sequences to extract building 3-D edges and organize them into planar regions. A knowledge-based model-driven approach subsequently reconstructed these regions as airtight models. Kwak and Habib [47] first detected the approximate boundaries of buildings from point cloud data. They then used a boundary matching strategy to improve model accuracy based on prior knowledge of right-angled roofs. Fan et al. [48] extracted roof ridgelines as the topological relationship between point cloud planes extracted in a data-driven manner and prior knowledge of gables' location, angle, and size. Zheng et al. [49] used a data-driven approach to detect roof step edges from LiDAR nDSM data and used this as the basis for roof type selection. Wu et al. [50] proposed a hybrid-driven method for indoor reconstruction from point cloud data. A data-driven strategy was used to extract feature points in the first step. In the second step, a model-driven strategy was used to detect an accurate layout, and the holes in the feature points were repaired. Finally, the structured points were converted into model data through Screened Poisson surface reconstruction. These hybrid-driven methods are strategies for combining prior knowledge and detection features for the whole input data in the linear process.

Inspired by the actual construction process and appearance of buildings, it is a common and practical idea to use the divide-and-conquer strategy for building models with complex structures. Lafarge and Mallet [51] constructed a large-scale urban model represented by a mixture of 3-D geometric primitives and mesh blocks. Song et al. [52] presented a primitive-based 3-D curved building reconstruction framework that segmented the point data into metamodels and refined the coarse primitives based on an embedded deformation graph. Fang et al. [53] divided the original triangular mesh data into structured scene mesh data and unstructured isolated object data when reconstructing indoor scenes and processed them separately to ensure the concise expression of the main scene and the delicate expression of nonmain objects simultaneously. These methods all use the divide-and-conquer strategy for bottom-up modeling. Using differentiation methods for building regions with diverse styles helps simplify the modeling difficulty and retain more detailed architectural characteristics. Still, they did not use the advantages of model-driven models. Zhang et al. [54] constructed a primitive library containing the primary roof surface model and superstructure and used a model-driven strategy for hierarchical reconstruction, but lacked the flexibility of the data-driven strategy. Satari et al. [55] used data-driven and model-driven methods to reconstruct the point cloud data of the main roof surface and dormer window region, respectively. However, they did not involve more prominent structure types and had poor scalability. To the authors' knowledge, this article is the first divide-and-conquer reconstruction method that implements data-driven and model-driven strategies for the different structures on the roof or façade with the mean of building surface mesh polygonization.

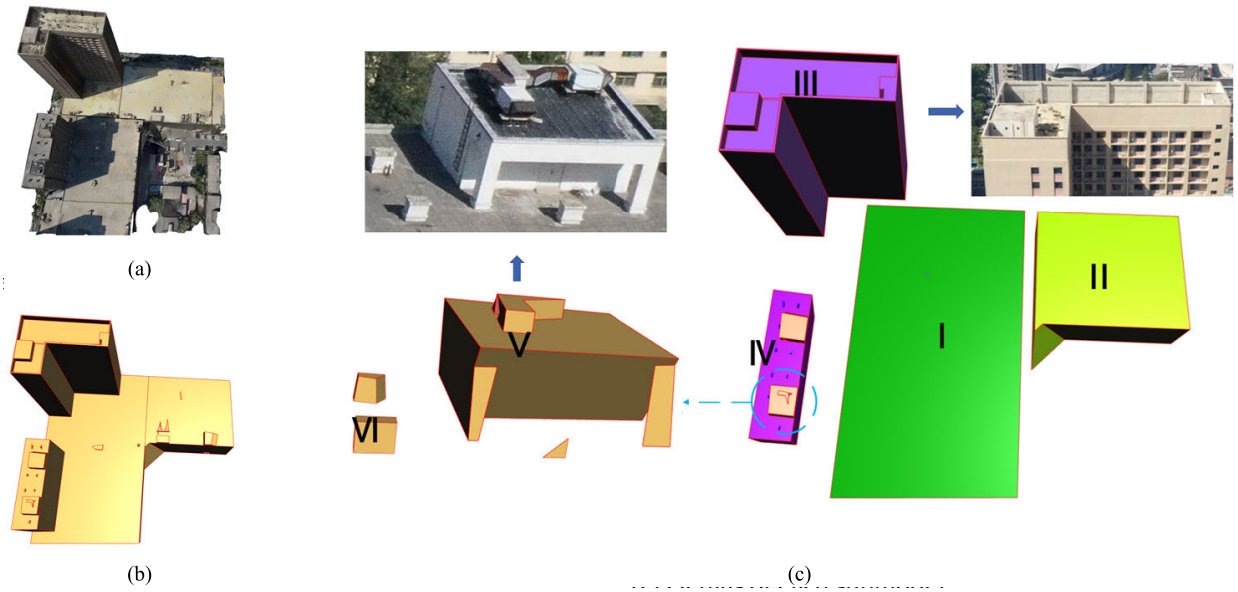

Fig. 1. Modeling results. The dashed arrow represents the close-up view of the circled area, and the solid arrows represent the corresponding UAV images. Colors and Roman numerals label the decoupled parts of the model. For ease of understanding, the ancillary structures attached to I and II are not shown in (c). (a) Colored mesh model. (b) Final result. (c) Details of each submodel.

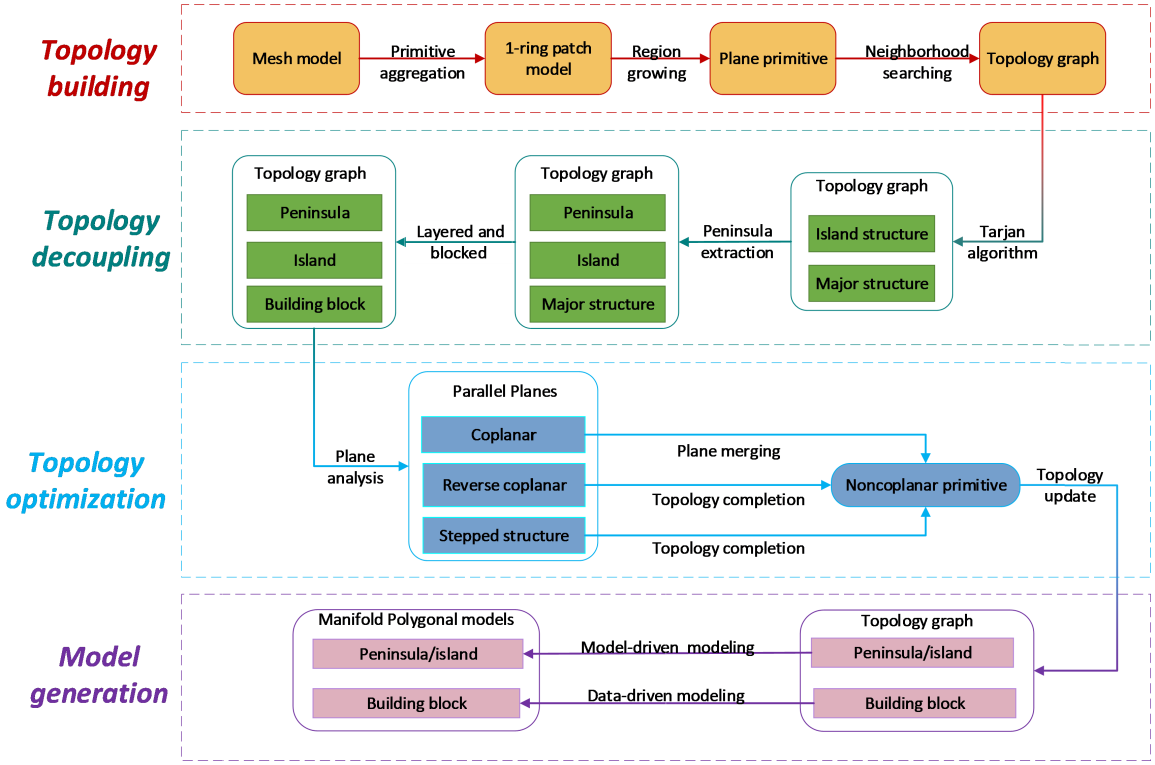

Fig. 2. Flowchart of the proposed method.

III. Methodology

A. Overview

The research in this article builds on our recent work UBMP-PaTo. Different from the data-driven method of UBMP-PaTo, this article adopts a hybrid-driven modeling method based on the divide-and-conquer strategy for urban building mesh polygonization, which we refer to as urban building mesh decoupling and polygonization (UBMDP) for short. Fig. 1 shows the visual realism of the component-based modeling results of UBMDP. Fig. 2 shows the pipeline of UBMDP, including the main processes of topology graph construction, topology decoupling, topology optimization, and model generation. We next highlight the main contributions of this article by contrasting it with the implementation details of UBMP-PaTo.

Section III-B: Roughly the same as UBMP-PaTo, this step also mainly goes through the 1-ring patch model transforming, region growing of primitives, and establishment of plane

region neighborhood relationships to build a plane topology graph. UBMP-PaTo has proved the efficiency and versatility of the 1-ring patch model, which is still adopted in this article. To ensure a more reasonable region-growing result, this article improves the normal calculation method of patch primitive.

Section III-C: This step is the core innovation of this article, and it is the premise to achieve hybrid-driven modeling. Topology decoupling, to establish a hierarchy, includes the main structure cut by building facades and roof planes and the island/peninsula-like structure extraction based on the Tarjan algorithm [56]. Both processes are carried out on topology graphs. Their commonality lies in finding one or two cutting planes as key topological nodes and obtaining relatively independent topology subgraphs through decoupling on graph nodes. Except for expanding the neighborhood relationship of the cutting plane in some cases, decoupling does not destroy the original topological relationship.

Section III-D: Due to the defects of raw data quality and the limitations of topology graph construction algorithms, improving model quality through topology optimization is an enduring postprocessing topic. SABMP merged nearly coplanar planes, UBMP-PaTo complemented the topological structure of the parapet, and this article further proposes more comprehensive optimizations of parallel planes.

Section III-E: The structure scale selects the data-driven or model-driven modeling strategy for the topology subgraph. For the main structures whose reconstruction targets are mainly facades and roofs, that is, the topological subgraphs obtained by cutting, this article adopts a data-driven strategy to perform the reconstruction. Although prior knowledge is also used for topology completion, the whole process is bottom-up. Finally, a polyhedral model is generated using the improved candidate face selection strategy in UBMP-PaTo. This article adopts a model-driven strategy to assist in model construction for the island or peninsula part where the reconstruction target is mainly a fine structure, and the detected planes are not completed. A simple geometric structure primitive library complements the missing subgraph nodes.

B. Topology Graph Construction

The topology graph is the restoration and encoding of the adjacency relationship between the building plane structures. Its construction needs to go through the process of primitive abstraction from the triangulation network, 1-ring patch, and then to the segmentation plane.

By converting the triangulation network into a set of 1-ring neighborhood aggregates and independent triangular faces, a more efficient expression of building surface morphology is realized. As shown in Fig. 3(b), each 1-ring patch is distinguished by different colors, and the independent triangular faces are labeled in black. To extract the plane primitives, our previous work designed an efficient region growth algorithm for 1-ring patches and used the distance and the angle included in the normal direction between the patch and the growth plane as indicators of the growth process. To ensure a more reasonable region growth result, this article uses the patch plane normal extracted by principal component analysis to replace the patch center point normal adopted in our previous work. The improved effect is shown in Fig. 3, where the extraction of the strip plane is more accurate. In the process of region growing, the adjacency relation of the plane can be determined according to that of 1-ring patches belonging to it. Taking plane primitives as graph vertices and connecting adjacent vertices with topology edges, we construct the undirected topology graph [as shown in Fig. 4(b)] which determines the relationship configuration between plane primitives and facilitates us to perform topology operations using the graph theory.

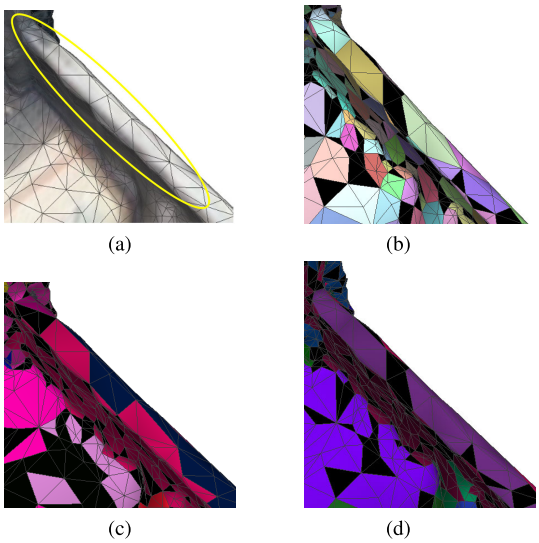

Fig. 3. Comparison of color-labeled region growing results. (a) Original model. (b) 1-ring patch model. (c) UBMP-PaTo [22]. (d) Improved result.

C. Topology Decoupling

As shown in Fig. 1, buildings in urban scenes often consist of the main structure (tall facades and horizontal roof datums) and attached delicate structures. When constructing a building polyhedron model, we generally use polygons with larger areas to represent the main structure of the building. Smaller area polygons are required for ancillary structures on roofs and facades, such as balconies, dormers, and chimneys. Using a single rule in plane extraction and topology construction is difficult to achieve the best quality of the two structures simultaneously. Many fine-structured planes would be lost when using a too-large region growing threshold. At the same time, a too-small one leads to fragmented results, which would reduce the efficiency of subsequent processing or even make the reconstruction fail. An obvious conclusion is that differentiated modeling strategies should be adopted for structures with nonnegligible scale gaps, and the ancillary structure should be distinguished from the main structure. In ancillary structure extraction, we proposed a strategy for separating strongly connected components of topology graphs based on the Tarjan algorithm and obtained subgraphs of island-like and peninsula-like regions.

In addition, the architecture paradigm and construction mode of urban buildings determine that buildings are generally present and distributed in layers and chunks. In the

vertical direction, the building mesh model can often be divided into roof regions, ground regions, and other layered regions by the horizontal plane. A building layer can also be cut into multiple independent chunks that are closely adjacent and relatively independent in the horizontal direction. By dividing the building into blocks, the complexity of the topology subgraph is reduced, and some reconstruction failures could be avoided. This process we call building layering and chunking.

1) Island/Peninsula Extraction: There are two primary forms of the fine structure attached to the main structure: 1) island-like regions and 2) peninsula-like regions. The island-liked region is only attached to the main plane and looks like an island in the building from the geometric appearance, so we call it an island vividly, such as the submodel VI in Fig. 1. The characteristic is that it is only connected to the main topology graph through one node. The peninsula-like region is attached to two planes, at least one of which is the major plane of the building, and looks like a peninsula extending from the main structure, such as the submodel V in Fig. 1. The characteristic is that it is only connected to the main topology graph by two topology nodes or one topology edge.

The extraction of the island/peninsula has three important implications as follows.

1) The spatial scale differences between the fine structure and the main structure make the degree of interference of data defects on the modeling quality different. It is more advantageous to deal with this issue based on the divide-and-conquer strategy.
2) The extracted independent structures generally have specific semantic attributes, such as dormers, bay windows, air conditioners, stacked sundries, and vegetation. The independence of submodels facilitates future application in editing and analysis.
3) The island/peninsula structure may introduce a ring structure in polygonization. Such nonsimple polygons will destroy the robustness of the geometric solution and increase the difficulty of geometric calculation and analysis, which should be avoided.

We adopt the Tarjan algorithm to extract island structures from the undirected adjacency graph of plane primitives. After the building topology graph is split at the cut point position, we select the topology subgraph with the most significant spatial scale as the main structure. The rest of the subgraphs are island structures in an attached position. The actual meaning of the cut point is the plane to which the island is attached, which is the only connection plane or cut plane between the island and the main structure. The schematic of the topological splitting process is shown in Fig. 4.

The peninsula region can also be called a double-connected region because of its two connection/cut planes. We restrict that the peninsula region should be the structure with actual semantics, and at least one of its connection planes is the building facade or roof datum plane. The building facade here refers to the vertical plane (height $>$ 3 m) adjacent to the ground extracted with the aggregation method proposed in UBMP-PaTo. The roof datum plane is not all the planes on the roof,

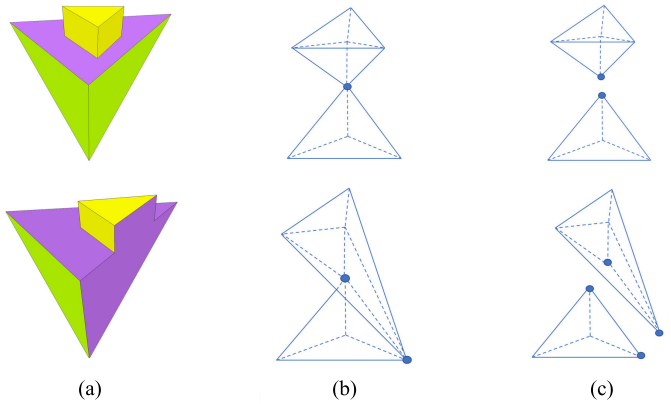

Fig. 4. (Yellow regions in the first row) Topological splitting of island structure and (yellow regions in the second row) peninsula structure. The purple planes in (a) are connection planes corresponding to the topology nodes in (b) and (c) highlighted in the blue dot.

but the principal plane of the roof with a large enough area ($>$9 m^2). The above planes are called candidate connection planes. Peninsula extraction is an iterative process. In each iteration, we first remove the topological node and its edge corresponding to one of the candidate connection planes and then execute the Tarjan algorithm to obtain the corresponding cut point and topology subgraph. After an iteration, whether the cut point is found or not, we add the connection plane back to the output topology graphs and continue the execution of another candidate plane. The candidate connection planes are removed by each search and the obtained cut-points are the two connected planes of the peninsula. The topology subgraph with a smaller spatial scale is the peninsula region. The schematic of the topological separation process is shown in Fig. 4.

2) Building Layering and Chunking: The facade and roof datum planes are the principal planes for building rendering and analysis. Using binary space partitioning to divide the building into layers and chunks at the main planes is in line with the actual construction law of buildings. It has great significance for the reconstruction and model application. In this article, layering refers to cutting a building with a horizontal plane, and chunking refers to cutting a building with a vertical plane.

The roof planes of buildings are sometimes discretely distributed in several building blocks that are closely connected by the façade. Building chunking is first performed to conform to the original topology graph. In Fig. 1, for example, block II is first cut out by chunking, and then blocks III and IV are separated by layering. The cutting plane of chunking is the building facade. The building chunking is essentially a cutting in geometric space. As a result, the model is divided into an upper submodel and a lower submodel according to the front and rear positional relationship between the plane regions and the cutting plane. We divide the planes to be cut into three categories: 1) upper planes; 2) lower planes; and 3) spanning planes. The upper plane and the lower plane, respectively, refer to the plane regions where all the patches are located on the front or back of the cutting plane. These planes are absorbed into the upper or lower subgraph, respectively. The spanning plane refers to the plane region where the cutting plane

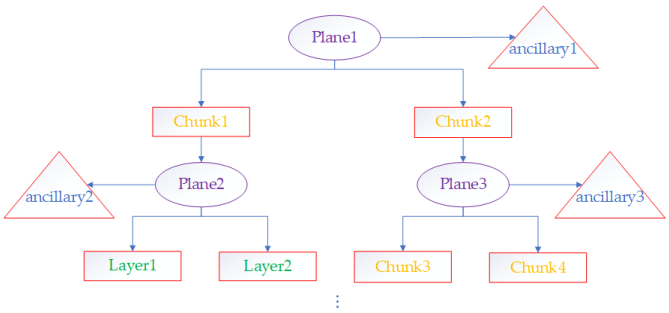

Fig. 5. Hierarchical topology graph.

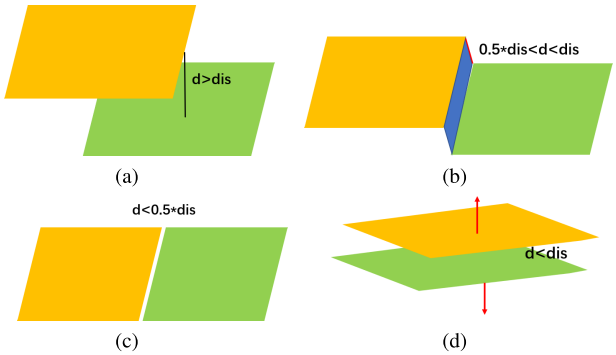

Fig. 6. Four parallel relationships. (a) Noncoplanar. (b) Stepped. (c) Normal coplanar. (d) Inverse coplanar.

crosses. It cannot simply be assigned to a certain subgraph for topological completeness. Resembling the cutting plane, the spanning plane belongs to the upper and lower subgraphs. The rooftop of submodels I and II in Fig. 1 is a spanning plane, and the chunking processing would not divide it into two planes. The discrepancy between the cutting plane and the spanning plane is that the former establishes a new adjacency relationship with all spanning planes. Building chunking is carried out in the order of the area of the building façade. If the number of topology subgraph nodes obtained by cutting is too few (<6), the current chunking would be canceled while the chunking of the following cutting plane continued.

Topology subgraphs obtained by building chunking continue to be layered. Compared with the rigid standard of the cutting façade to be adjacent to the ground, the horizontal plane on which the building is layered is selective. Compromising the difficulty to judge the actual floor distribution of buildings from mesh data, the main focus of building layering is put on the large-area horizontal cut planes with significant upper and lower stratification. Building layering is an iterative process from low to high. We take the bottom surface of the building block bounding box as the reference and select the lowest horizontal plane with a large area ratio (>5%) and a sufficiently significant height difference (>3 m) as the candidate cut plane. If the upper topology subgraph obtained by cutting has enough nodes (>5), update the bounding box for the next round of layering. Otherwise, select a higher plane to try layering.

As shown in Fig. 5, the result of topology decoupling is a hierarchical topology graph. The connection plane separates the original topology graph into subgraphs: layers, chunks, and ancillary structures. In actual implementation, these two steps are alternated, i.e., the ancillary structure extraction step is interspersed before and after the iteration process of layering and chunking.

D. Parallel Plane Topology Optimization

The accurate plane extraction result and the correct plane relationship directly impact the modeling results. We summarize the parallel properties of the extracted plane regions into four categories: 1) noncoplanar parallel planes; 2) stepped plane pairs; 3) normal coplanar planes; and 4) inverse coplanar planes, as shown in Fig. 6. Parallel planes here refer to a couple of planes whose included angle between the plane normals is less than 10° or greater than 170°. Noncoplanar parallel planes refer to parallel planes whose plane distance exceeds the distance threshold dis, and there is no adjacency relationship between them. Following equation is the calculation formula of the distance threshold dis:

$$\text{dis} = \sum_{i=0}^{n} l_i/(n * c) \tag{1}$$

where l_i is the length of edge i of the triangular network, n is the number of edges in the triangular network, and c is the adjustment coefficient, which defaults to 1.

For a correct topology graph, adjacency and parallelism are not allowed to exist between two planes simultaneously. However, due to errors in the results of region growing, a mass of adjacent parallel planes exists. They are mainly manifested in stepped adjacency, normal coplanarity, and inverse coplanarity. Parallel planes coplanar means that the distance from a plane region to its parallel plane is less than the threshold dis. If coplanar parallel planes' normals face opposite directions, the pair of planes is inverse coplanar. Coplanar parallel plane pairs with the same normal orientation can be further subdivided into the stepped relationship and normal coplanar relationship, where the distance between the normal coplanar planes is less than $0.5 * \text{dis}$, and the distance between the stepped plane pair is between $0.5 * \text{dis}$ and dis. We formulate different optimization strategies for these plane relationships.

In our previous work UBMP-PaTo, the inverse coplanar plane has already caught our attention. This structural property is generally manifested as parapets, thin walls, and billboards, in buildings. The targeted topology optimization in UBMP-PaTo is effective, and this method continues to be used in this article. In the case of continuous inverse coplane where a mid-plane is adjacent to and parallel to two noncoplanar parallel planes, we adjust the mid-plane normal to make it 45° to its two parallel planes, as the plum red plane shown in Fig. 7. As the normal coplanar plane pair is essentially a plane, we merged them as designed in UBMP-PaTo.

The optimization of stepped plane pairs is one of the most notable contributions of this article. Normal coplanar planes exist due to over-segmentation and a plane region is divided into multiple ones in the setting of a relatively small growth threshold. The stepped plane pair is induced by a fairly large growth threshold when two parallel planes that are not adjacent establish an adjacency relationship across their midplane.

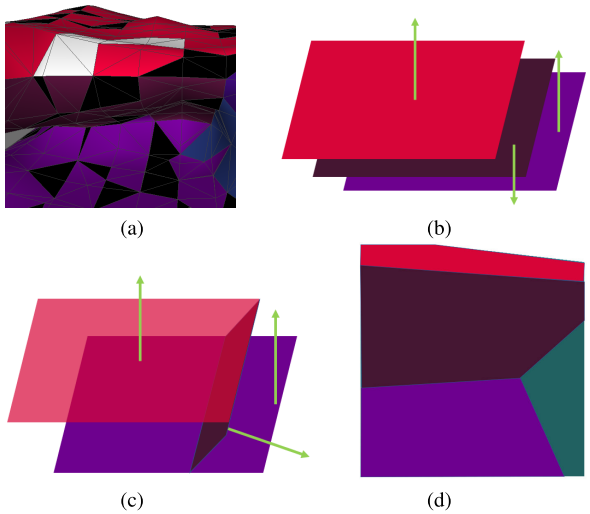

Fig. 7. Continuous inverse coplanar plane topology optimization. The same plane is identified with the same color. (a) Plane extraction results. (b) Initial plane relationship. (c) Adjusted plane. (d) Model structure.

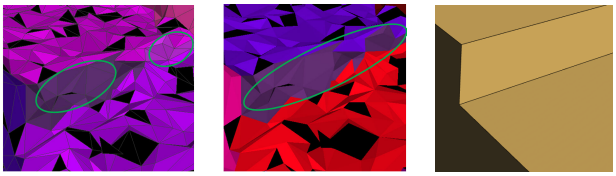

Fig. 8. Stepped structure topology optimization. The green circle means the mid-plane. (a) Raw growth result. (b) Midplane merging. (c) Model structure.

The two cases are not distinguished in UBMP-PaTo, which leads to the result of plane under-segmentation. More seriously, the coplanar plane merging is an iterative update process of the plane equation, and the continuous merging of continuously stepped planes will lead to an increasing error accumulation.

To eliminate the error accumulation phenomenon and obtain a finer planar structure, we remove the adjacency of two parallel planes and restore the mid-plane structure. The so-called mid-plane refers to the connecting plane region between two parallel planes, usually presenting an elongated strip-shaped structure. The initial extraction results of the mid-plane obtained by region growing are easily affected by the noise and exhibit broken and incomplete structures. We have formulated the following topology optimization rules in a targeted manner.

1) Robustly merge these broken mid-planes using a loose criterion to support the stepped structure with the fewest mid-planes, as shown in Fig. 8.
2) For the mid-plane with an unstable neighborhood structure (neighborhoods < 4), traverse other mid-plane regions, calculate the nearest distance from this plane region to the traversed plane, and select the plane with the smallest distance to join the neighborhoods.
3) Cancel the neighborhood relationship between two parallel planes.

TABLE I
ANCILLARY STRUCTURE PRIMITIVE MODEL LIBRARY

Primitive	Standard structure	To be complemented
Cuboid		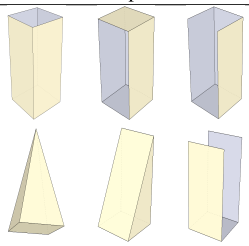
Triangular prism	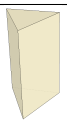	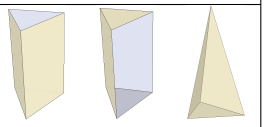

E. Hybrid-Driven Modeling

The hybrid-driven modeling strategy is the most significant difference between UBMDP and other mesh polygonization methods. That is to say, both data-driven and model-driven ideas are used in the modeling process to overcome their respective shortcomings.

1) Model-Driven Island/Peninsula Modeling: Due to the smaller spatial scale of the ancillary structures of buildings, the topological quality of islands and peninsulas under the same growth threshold is relatively poor, and it is difficult to obtain satisfactory modeling quality directly with data-driven methods. Therefore, on the premise that these fine structures have been decoupled, we have the opportunity to use a model-driven method to make up for data defects.

Considering the difficulty of defining all fine structures with a set of primitive libraries and the ubiquity of simple ancillary structures in buildings, island/peninsula structures with too many topology nodes (>5) are still reconstructed using the data-driven approach in the actual implementation process. Other simple ancillary structures, such as dormers, and balconies, are most likely to fail to obtain a closed model due to missing topology or inaccurate plane extraction. The loss of plane topology caused by under-segmentation and the plane distortion caused by inaccurate segmentation make model-driven methods more suitable. Thus, we constructed a simple geometry primitive library for ancillary structures of buildings in Table I.

As can be seen from Table I, our primitive library is quite simple, covering only the most common building ancillary structures: cuboids and triangular prisms. The primitive library does not contain slightly more complex geometries (such as pentagonal prisms) or even quadrangular and triangular pyramids with fewer facets. The pentagonal prism structure can be reconstructed in a data-driven manner without going through a model-driven process. In addition, the detected pyramid structures are often prisms missing a top face, and the reconstruction of actual pyramid structures as prisms would not lose too much information. In conclusion, the most critical purpose of the model-driven strategy is to ensure legal topology and watertight geometry, and the loss of details is unavoidable.

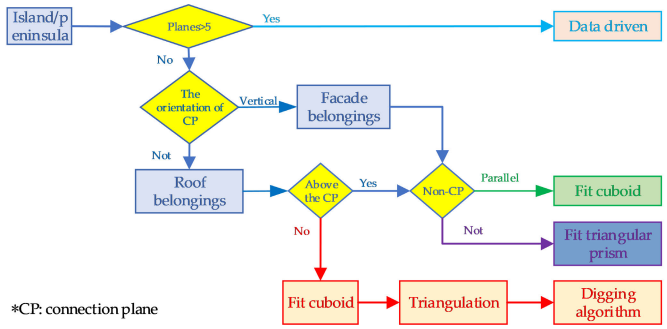

Fig. 9. Stepped structure topology optimization. The green circle means the mid-plane.

As shown in Fig. 9, we set some judgment rules to fit the primitive library model, such as the number of planes, the direction of connection planes, and the parallel relationship of nonconnection planes. Corresponding model fitting rules are designed for belongings of the facade, flat roof, and sloping roof. The model fitting process adopts the means of soft constraints that only the incomplete part of the original structure is complemented, and other parts are not required to comply with matching primitive. The specific fitting rules are straightforward and trivial, and it is not necessary to elaborate on them. It should be noted that the above rules are designed for prominent structures. For the concave island/peninsula structure below the roof, we use the Boolean operation to dig a hole in the main structure is referred to as the digging algorithm.

2) Data-Driven Model Generation: For the main structure and the ancillary structure with more than five planes, this article adopts the data-driven polygon model generation strategy in UBMP-PaTo. Some targeted improvements are made to cope with the special properties engendered by topology decoupling.

Polyhedral model generation mainly includes two steps: structural feature extraction and candidate face optimization. The structural features include structure points generated by the intersection of three adjacent proxy planes and structure lines generated by two adjoining proxy planes. As each independent model is a further subdivision of the original building space, the bounding boxes of the independent model replace that of the whole building to constrain the structural points and structural lines. This improvement can further avoid the appearance of illegal spikes in the model.

The candidate's face is a polygon representing a plane region formed by feature points and feature lines through projection and arrangement processes. To eliminate the influence of topology errors on the water-tightness and manifoldness of the simplified model, we adopted the binary linear programming method in SABMP to optimize the candidate faces. Since the cutting planes belong to the upper and lower subgraphs at the same time after layering and chunking, and the adjacency relationship with the spanning planes is additionally established, topology problems arise spontaneously, which may directly lead to the failure of model construction. As shown in Fig. 10(d), the annular region is incorrect due to the redundant

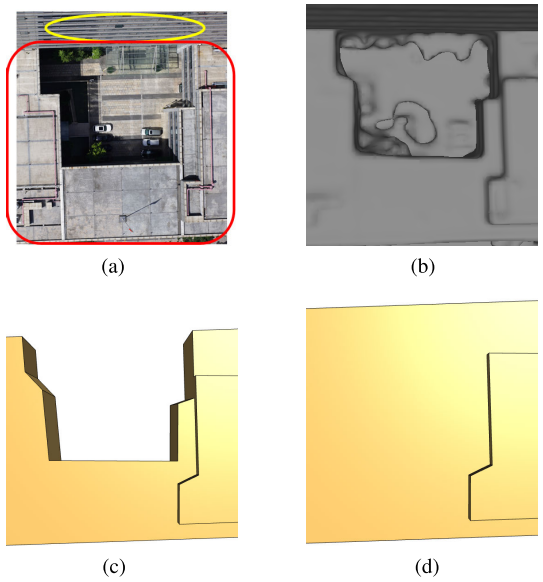

Fig. 10. Significance of screening candidate faces for cutting planes. The red circle is the building block to be reconstructed, and the yellow circle is the cutting plane. UBMDP is the abbreviation of our method. (a) Reference image. (b) Original mesh. (c) UBMDP model. (d) No screening.

presence of the cutting plane. Only by deleting the unnecessary candidate face of the cutting plane in advance (yellow circle in Fig. 10) the modeling result can conform to the actual building structure [Fig. 10(c)]. The deletion conditions we add to constrain the cutting plane are shown as follows:

$$\text{Area}\left(M_i^a\right) > 0.6 * \text{Area}(f_i), \quad f_i \epsilon F_{\text{low}}. \tag{2}$$

In this formula, f_i represents the candidate face, M represents the simplified model, M_i^a represents the part covered by the original mesh, F_{low} represents the candidate face set formed by the subgraph on the cutting plane, and 0.6 is the empirical parameter.

IV. Results

The UBMDP method has been implemented based on UBMP-PaTo, and the programming language used was C++. The topological operations (such as the Tarjan algorithm) involved in this article were done using the Boost library [57], and the CGAL library [58] was mainly used for geometric calculations. In addition, we used easy3D [59] for polygon model rendering. Through qualitative and quantitative analysis of different experimental data, the UBMDP method validated its advantages over other relevant methods.

A. Qualitative Analysis

The UBMDP method is suitable for polygonizing single-building mesh models containing ground regions and can be directly applied to monomer buildings extracted manually or automatically. In Fig. 11, we conducted experiments with eight photogrammetric mesh models containing various forms of noise distributed on the ground and building regions. The Poisson Reconstruction method generated the mesh model a), b), g), and h) from the dense point cloud. Model g) and h) were derived from the same piece of point cloud data,

TABLE II
REASONS FOR MODEL QUALITY IMPROVEMENT

Model	a)	b)	c)	d)	e)	f)	g)	h)
Topology optimization	×	✓	✓	×	✓	✓	✓	×
Topology decoupling	✓	✓	×	✓	✓	✓	×	✓

TABLE III
ADJUSTABLE PARAMETERS USED IN THE THREE METHODS

Model		a)	b)	c)	d)	e)	f)	g)	h)
SABMP	c_d	0.8	0.5	1	0.9	0.9	0.35	0.6	0.6
	c_a	0.3	0.1	0.2	1	0.5	0.1	0.1	0.3
UBMP-PaTo	c	1	1	1	1	1	0.5	1	1
UBMDP	c	1	1	1	1	1	1	1	1

while h) with greater reconstruction density. Model f) was generated from images using ContextCapture, while GodWork generated the mesh model of Fig. 1. Models c), d), and e) were from the open-source dataset. The UBMDP method results in multiple independent submodels, including the main structure and island/peninsula models. Each submodel is a polygonal model with an excellent compression ratio and guarantees water-tightness and manifoldness, which is different from the classical mesh decimation method (such as the QEM method in Fig. 11). The submodels are closely combined by connection planes to form a building model with high structural integrity.

The model results in Fig. 11 shows that the UBMDP method has more detailed structural information than the other mesh polygonization methods, such as SABMP and UBMP-PaTo. Topology decoupling plays a significant role in improving model quality. The quality improvement of model a) is mainly due to the digging algorithm, and the modeling of prominent structures improves the quality of model e). The quality improvement of model c) is primarily due to the topology optimization of the stepped parallel planes. The sets of close-ups in Fig. 12 highlight where the quality improvement occurs. Table II detailed the reasons for the improved quality of each model. By comparing with the reference image, we can find that the models generated by UBMDP are closer to the actual building shape. This conclusion applies to the sloped roof building d) and the flat roof building h), high noise data e) and low noise data f), low-rise buildings c) and high-rise buildings b).

The UBMDP method has an adjustable parameter c. The smaller the coefficient c, the larger the growth threshold, and the rougher the final result, which is the same as UBMP-PaTo. SABMP tunes two thresholds to get the best modeling results: a distance threshold c_d that determines the region growing step and an area threshold c_a that screens the plane. The thresholds used in the eight groups of data are shown in Table III. It can be seen that UBMDP is less dependent on parameter adjustment.

B. Quantitative Analysis

The ability to compress the data file is an important index to evaluate the performance of the mesh simplification algorithm. Table IV shows that the file compression ratio of UBMDP is roughly between 0.11% and 0.75%, depending on the quality of the original data and the actual complexity of the building structure. The corresponding face contraction ratio is between 0.06% and 0.37%. The file compression ratio of the other two methods is smaller than that of UBMDP, a tradeoff that must be made to preserve the important structural characteristics of the building.

Hausdorff distance is a standard index to evaluate the similarity of two geometric models [61]. This article used the original model as a sampling/reference mesh. The Hausdorff distance to the simplified model was calculated to evaluate the ability to preserve the structure of the original model. When the sampling points of the original model can find neighboring points with smaller distances on the simplified model, which means a superior ability to maintain the structure, the algorithm manifests a lower root mean square (rms) value of the Hausdorff metric. Since polygonization methods focus on the lightweight representation of building regions, we roughly removed the nonbuilding region data of the original model before quality evaluation, as shown in Fig. 13.

This article compares the structure retention ability of six methods aimed at simplifying the representation of the building surface. Fig. 14 visualizes the Hausdorff distance and the overall rms index of the model. The first and second small rms values are highlighted in bold. QEM, VSA, and SAMD are all classical mesh decimation methods. Inferior to polyhedron methods such as SABMP, UBMP-PaTo, and UBMDP, they cannot guarantee manifoldness and water-tightness.

As shown in Fig. 15, compared to the polyhedron method's remarkable feature representation ability and realism, the results of the mesh decimation method, aiming at local optimization, were full of fragmentary information, which cannot well reflect the real structure. For fairness, we used these three methods to reduce the input data to the same degree as the number of vertices in the UBMDP result. Through the quantitative analysis of the modeling quality, we found that the UBMDP method has excellent modeling quality, and the top six models have achieved the first or second ranking. The rms value of UBMDP is slightly inferior to that of QEM and SAMD only when dealing with large-area simple flat-roofed buildings under the same vertex contraction target. The cause is that the main structure of the building f) needs relatively few feature points. Using the traditional mesh decimation method will not lead to too much loss of structural information but can better preserve the unstructured surface. When faced with buildings with complex geometric structures, the rms values obtained by the UBMDP method are the smallest among the six methods, such as models a)–d). Compared with other polyhedral methods, UBMDP consistently achieves the best rms value, the same as the previous analysis results. Further considering the simplified results' manifoldness, water-tightness, and polygonization, we believe UBMDP to achieve state-of-the-art performance in the structure-aware reconstruction of building mesh data.

V. DISCUSSION

A. LoD3 Reconstruction Capability

Benefiting from the ability of topology decoupling to model the ancillary structures separately, the UBMDP algorithm has

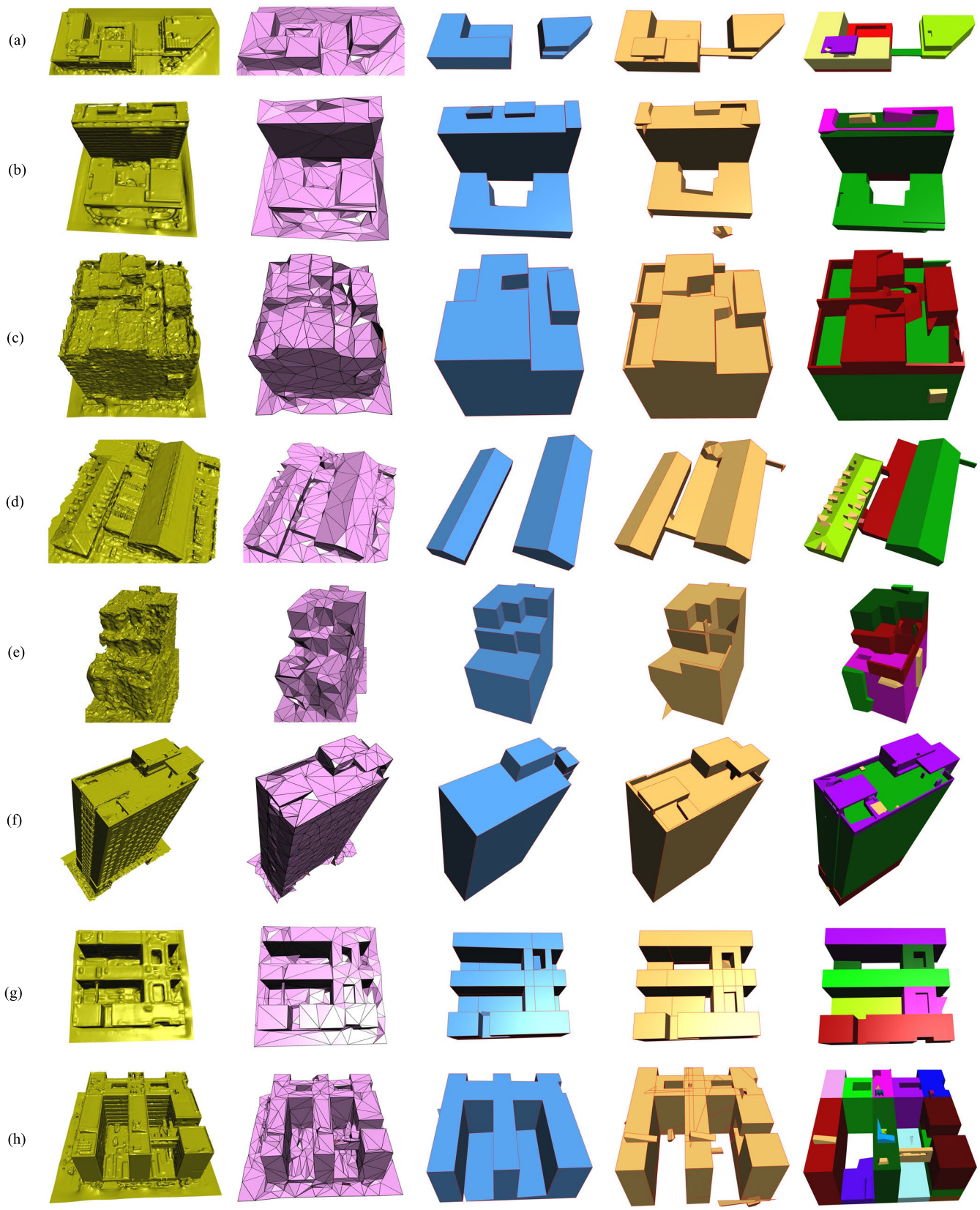

Fig. 11. (a)–(h) Comparison of modeling results. From left to right are the original mesh model, QEM [38] result, SABMP [45] result, UBMP-PaTo result, and our UBMDP result. Colors distinguish the submodels in the UBMDP results.

TABLE IV
FILE COMPRESSION RATIO

Model		a)	b)	c)	d)	e)	f)	g)	h)
original file size (MB)		4.08	3.40	1.90	1.54	1.77	15.6	3.41	16.6
SABMP	file size (KB)	1.58	2.74	1.81	1.24	1.90	1.83	4.58	2.76
	compression ratio (%)	0.04	0.08	0.10	0.08	0.11	0.01	0.13	0.02
UBMP-PaTo	file size(KB)	3.50	4.83	4.01	3.35	3.17	4.78	4.47	14.1
	compression ratio (%)	0.09	0.14	0.21	0.22	0.18	0.03	0.13	0.08
UBMDP	file size(KB)	9.47	8.71	9.62	11.5	9.02	30.7	8.53	18.3
	compression ratio (%)	0.23	0.26	0.51	0.75	0.51	0.20	0.25	0.11
	face contraction (%)	0.17	0.18	0.30	0.37	0.37	0.10	0.18	0.06

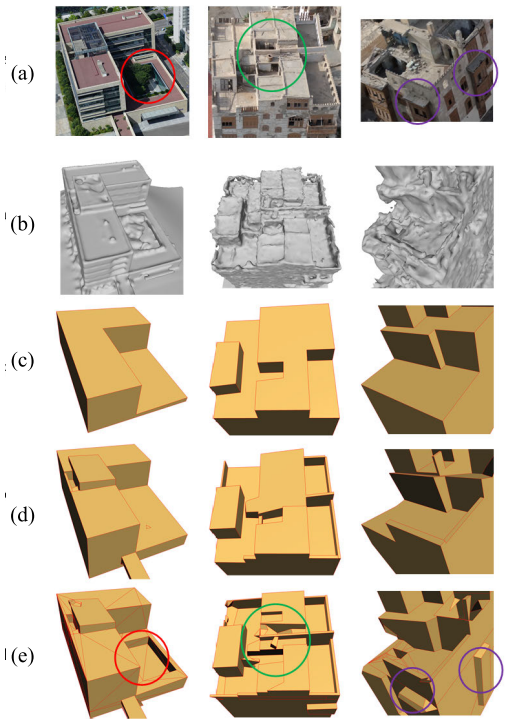

Fig. 12. Close-up of the dramatic increase in model quality. The image source in the second and third columns are provided by Nan [60]. (a) Image source. (b) Origin mesh. (c) SABMP. (d) UBMP-PaTo. (e) UBMDP.

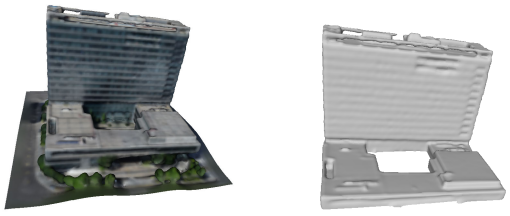

Fig. 13. Reference mesh with only the building region. (a) Origin mesh model. (b) Reference mesh.

a certain LoD3 reconstruction ability. The LoD3 model refers to the building model including detailed architecture, while the LoD2 model only has a complex roof and simple facade. The LoD3 reconstruction capability refers to the function of reconstructing the building's detailed structure such as windows, balconies, and chimneys. UBMDP constructs a hierarchy topology graph and determines the level of details according to whether to output the ancillary submodel. Fig. 16(a) is a part of the LoD2 model of data d), Fig. 16(b) is the LoD3 model, including the detailed structure of the roof surface such as dormers and chimneys, and Fig. 16(c) is the LoD2 model of the bottom part of data e). Fig. 16(d) is the LoD3 model containing the detailed structure of the facade. At present, the representation of doors and windows is not covered by our method.

B. Efficiency

The efficiency of mesh simplification is an essential factor in evaluating the practicability of the algorithm. Fig. 17 counts the time spent by the six methods mentioned above to obtain the results shown in Fig. 14. The experiment platform is a mobile workstation with a 2.30 GHz Intel[1] Core[2] i9-9880H CPU and 64 GB RAM. Comprehensive analysis shows that QEM has the highest efficiency as a classical mesh decimation algorithm. SABMP and SAMD have much higher running times than other algorithms due to their structure-aware properties and are an order of magnitude slower than QEM. The running time of VSA and UBMP-PaTo are slightly higher than QEM, basically at a comparable level. Due to the complexity of topology processing and the enrichment of geometric structures, the processing time required by UBMDP is roughly two to three times that of QEM, which is still in the same order of magnitude and has apparent advantages over SABMP and SAMD. The efficiency of UBMDP is about half that of UBMP-PaTo, which is a reasonable tradeoff for better polyhedral model results. The efficient performance of UBMDP reflects its competitiveness and applicability.

C. Limitation

Limited by the quality of the data itself and the targeted algorithm design, although the UBMDP method has taken a big step in the polygonization of building mesh data considering structural recovery, there are still some shortcomings. On the one hand, UBMDP is only applicable to reconstructing a single building. For simple composite building regions such as model a) and model d), the result of the monolithic model we obtained is ideal. However, for larger-scale building groups, more complex plane primitive relationships and exponentially increasing spatial computation are unpredictable for the current UBMDP method. Faced with this kind of data, the preextraction step of building singulation is necessary. On the other hand, the fixed-threshold plane extraction strategy and

[1]Registered trademark.
[2]Trademarked.

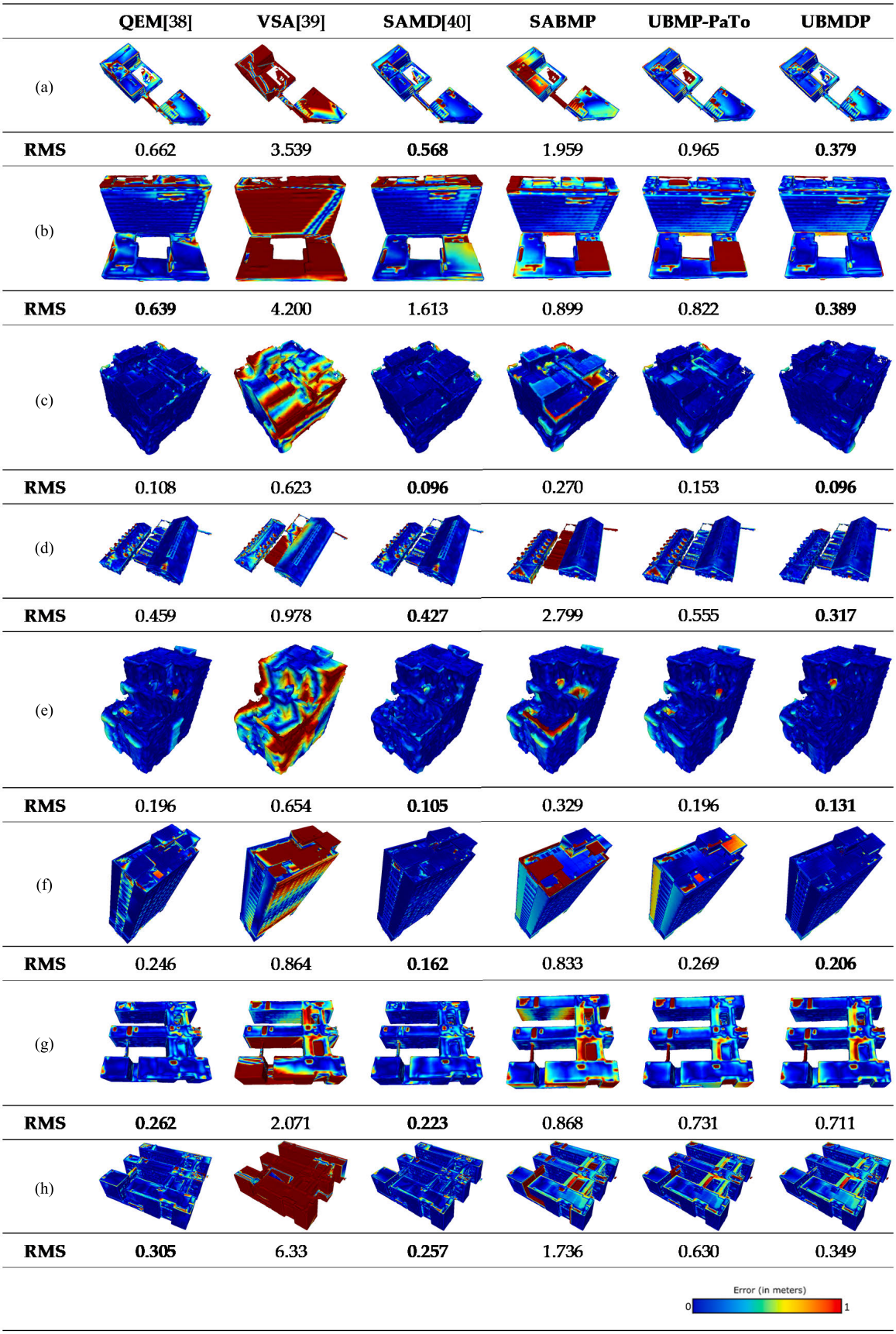

Fig. 14. Comparison of building structural retention capability.

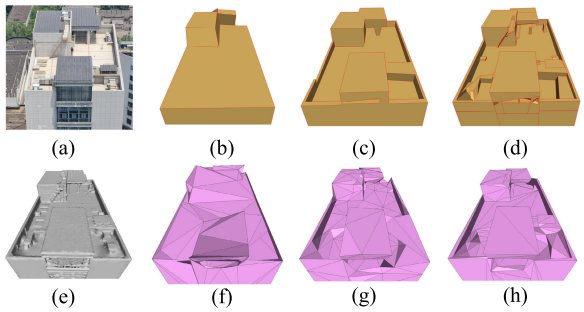

Fig. 15. Comparison of (b)–(d) polyhedron and (f)–(h) nonpolyhedron methods. (a) Reference image. (b) SABMP. (c) UBMP-PaTo. (d) UBMDP. (e) Origin mesh model. (f) VSA. (g) QEM. (h) SAMD.

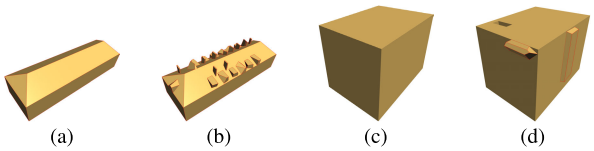

Fig. 16. LoD2 and LoD3 modeling results for UBMDP.

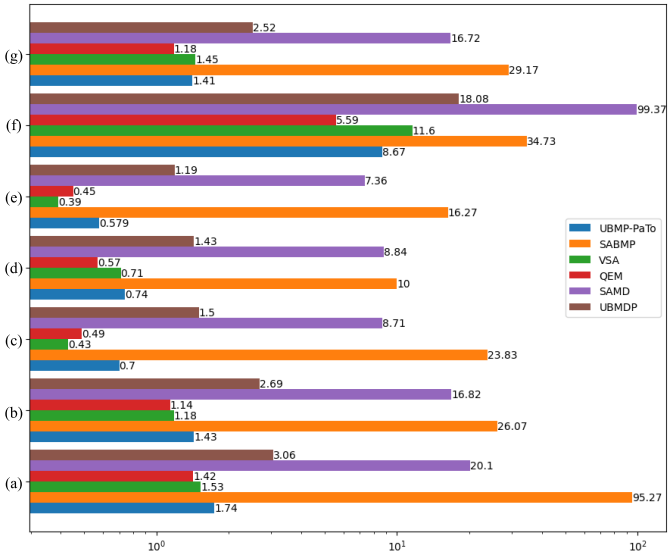

Fig. 17. Running time comparison.

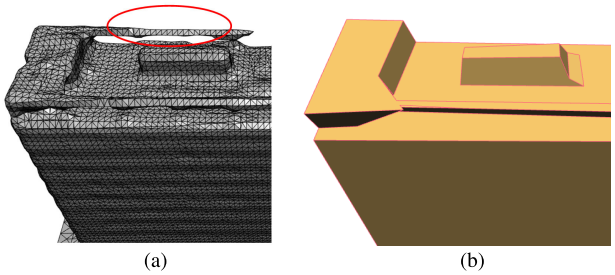

Fig. 18. Unstructured mesh data modeling results. (a) Origin mesh. (b) Model result.

the topology optimization rules for segmented plane structures make UBMDP unpredictable when faced with unstructured surface reconstruction. As shown in the complex structure in the red circle in Fig. 17, its mesh model shows an irregular surface shape, and the modeling result in this area is not satisfactory.

VI. Conclusion

We propose a hybrid-driven reconstruction strategy capable of topology decoupling and polygonization based on urban building mesh models. Topology decoupling involves building layering, chunking, and ancillary structure separation, resulting in relatively independent topology subgraphs that maintain spatial adjacency through connection planes. A data-driven modeling strategy is implemented after topology optimization of the main structure, especially its parallel planes. A model-driven modeling strategy is implemented for the ancillary structure based on the topology completion library. The primary function of topology decoupling is to select appropriate modeling rules according to the characteristics of submodels. The final result of our method is a set of submodels, and each of them is a lightweight polyhedron model with watertight and manifold properties. Using the obtained model set and its affiliation, we can choose to output the LoD2 model or the LoD3 model as needed, providing a flexible and efficient data type for tasks such as 3-D geometric calculation, spatial analysis, and scene interaction. In terms of building structure retention ability, UBMDP outperforms other polyhedron methods. Its consistency with the original mesh is also first-class compared with nonpolyhedron methods. In terms of efficiency, UBMDP is competitive, and its slightly higher processing time than QEM would not limit its practicality. Our research is meaningful for promoting real 3-D city model reconstruction and enriching model applications.

Our research has many possibilities waiting to be discovered. In terms of model-driven strategies, we can consider adding a primitive library of parametric models to deal with curve surface regions, such as cylinders and cones. Moreover, incorporating a learning-based approach in our research is also expected to improve modeling performance. For example, graph neural network-based topology optimization and convolutional neural network-based window extraction are all work we hope to complete in the future.

Acknowledgment

The authors would like to thank Liangliang Nan and Yawen Liu for their help in providing some experimental data.

References

[1] N. Haala and M. Kada, "An update on automatic 3D building reconstruction," *ISPRS J. Photogramm. Remote Sens.*, vol. 65, no. 6, pp. 570–580, Nov. 2010.

[2] M. Berger et al., "A survey of surface reconstruction from point clouds," *Comput. Graph. Forum*, vol. 36, no. 1, pp. 301–329, Jan. 2017.

[3] F. Biljecki, J. Stoter, H. Ledoux, S. Zlatanova, and A. Çöltekin, "Applications of 3D city models: State of the art review," *ISPRS Int. J. Geo-Inf.*, vol. 4, no. 4, pp. 2842–2889, Dec. 2015.

[4] W. Li, L. Meng, J. Wang, C. He, G. Xia, and D. Lin, "3D building reconstruction from monocular remote sensing images," in *Proc. IEEE/CVF Int. Conf. Comput. Vis. (ICCV)*, Oct. 2021, pp. 12528–12537.

[5] T. Rakha and A. Gorodetsky, "Review of unmanned aerial system (UAS) applications in the built environment: Towards automated building inspection procedures using drones," *Autom. Construct.*, vol. 93, pp. 252–264, Sep. 2018.

[6] *OpenMVS: Multi-View Stereo Reconstruction Library*. [Online]. Available: https://github.com/cdcseacave/openMVS

[7] E. K. Stathopoulou and F. Remondino, "Open-source image-based 3D reconstruction pipelines: Review, comparison and evaluation," in *Proc. 6th Int. Workshop Lowcost 3Dsensors, Algorithms, Appl.*, 2019, pp. 331–338.

[8] C. Griwodz et al., "AliceVision meshroom: An open-source 3D reconstruction pipeline," in *Proc. 12th ACM Multimedia Syst. Conf.*, Jun. 2021, pp. 241–247.

[9] *Agisoft Metashape*. [Online]. Available: https://www.agisoft.com/

[10] *Contextcapture | 3D Reality Modeling Software | Bentley*. [Online]. Available: https://www.bentley.com/en/products/brands/contextcapture

[11] *Ramap Technology*. [Online]. Available: http://www.uavmap.cn/

[12] J. Junhui, H. Ming, and L. Xianglei, "Surface reconstruction algorithm based on 3D Delaunay triangulation," *Acta Geodaetica et Cartographica Sinica*, vol. 47, no. 2, p. 281, 2018.

[13] M. Kazhdan and H. Hoppe, "Screened Poisson surface reconstruction," *ACM Trans. Graph.*, vol. 32, no. 3, pp. 1–13, Jun. 2013.

[14] W. E. Lorensen and H. E. Cline, "Marching cubes: A high resolution 3D surface construction algorithm," *ACM SIGGRAPH Comput. Graph.*, vol. 21, no. 4, pp. 163–169, Aug. 1987.

[15] S. Yao, J. Zhang, Z. Hu, Y. Wang, and X. Zhou, "Autonomous-driving vehicle test technology based on virtual reality," *J. Eng.*, vol. 2018, no. 16, pp. 1768–1771, Nov. 2018.

[16] L. Xing, B. Jiao, Y. Du, X. Tan, and R. Wang, "Intelligent energy-saving supervision system of urban buildings based on the Internet of Things: A case study," *IEEE Syst. J.*, vol. 14, no. 3, pp. 4252–4261, Sep. 2020.

[17] A. M. Aburbeian, A. Y. Owda, and M. Owda, "A technology acceptance model survey of the metaverse prospects," *AI*, vol. 3, no. 2, pp. 285–302, Apr. 2022.

[18] D. Che, Z. Li, Y. Liu, R. Zhong, and B. Ma, "A new method of achieving single three-dimensional building model automatically based on oblique photography data," *Math. Problems Eng.*, vol. 2021, pp. 1–12, Sep. 2021.

[19] J. Han et al., "Urban scene LOD vectorized modeling from photogrammetry meshes," *IEEE Trans. Image Process.*, vol. 30, pp. 7458–7471, 2021.

[20] L. Zhu, S. Shen, X. Gao, and Z. Hu, "Large scale urban scene modeling from MVS meshes," in *Computer Vision—ECCV 2018*. Cham, Switzerland: Springer, 2018, pp. 640–655.

[21] *CityGML*. [Online]. Available: http://www.opengeospatial.org/standards/citygml

[22] L. Yan, Y. Li, and H. Xie, "Urban building mesh polygonization based on 1-ring patch and topology optimization," *Remote Sens.*, vol. 13, no. 23, p. 4777, Nov. 2021.

[23] T. Feng, F. Fan, and T. Bednarz, "A review of computer graphics approaches to urban modeling from a machine learning perspective," *Frontiers Inf. Technol. Electron. Eng.*, vol. 22, no. 7, pp. 915–925, Jul. 2021.

[24] P. Musialski, P. Wonka, D. G. Aliaga, M. Wimmer, L. van Gool, and W. Purgathofer, "A survey of urban reconstruction," *Comput. Graph. Forum*, vol. 32, no. 6, pp. 146–177, Sep. 2013.

[25] R. Wang, J. Peethambaran, and D. Chen, "LiDAR point clouds to 3-D urban models: A review," *IEEE J. Sel. Topics Appl. Earth Observ. Remote Sens.*, vol. 11, no. 2, pp. 606–627, Feb. 2018.

[26] H.-G. Maas and G. Vosselman, "Two algorithms for extracting building models from raw laser altimetry data," *ISPRS J. Photogramm. Remote Sens.*, vol. 54, nos. 2–3, pp. 153–163, Jul. 1999.

[27] F. Lafarge, X. Descombes, J. Zerubia, and M. Pierrot-Deseilligny, "Structural approach for building reconstruction from a single DSM," *IEEE Trans Pattern Anal Mach Intell*, vol. 32, no. 1, pp. 135–147, Nov. 2010.

[28] B. Xiong, S. O. Elberink, and G. Vosselman, "A graph edit dictionary for correcting errors in roof topology graphs reconstructed from point clouds," *ISPRS J. Photogramm. Remote Sens.*, vol. 93, pp. 227–242, Jul. 2014.

[29] Z. Li and J. Shan, "RANSAC-based multi primitive building reconstruction from 3D point clouds," *ISPRS J. Photogramm. Remote Sens.*, vol. 185, pp. 247–260, Mar. 2022.

[30] F. Rottensteiner and C. Briese, "Automatic generation of building models from LiDAR data and the integration of aerial images," in *Proc. ISPRS*, vol. 34, 2003.

[31] X. Wen, H. Xie, H. Liu, and L. Yan, "Accurate reconstruction of the LoD3 building model by integrating multi-source point clouds and oblique remote sensing imagery," *ISPRS Int. J. Geo-Inf.*, vol. 8, no. 3, p. 135, Mar. 2019.

[32] G. Sohn, Y. Jwa, J. Jung, and H. Kim, "An implicit regularization for 3D building rooftop modeling using airborne LiDAR data," *ISPRS Ann. Photogramm., Remote Sens. Spatial Inf. Sci.*, vols. I–3, pp. 305–310, Jul. 2012.

[33] M. Li, P. Wonka, and L. Nan, "Manhattan-world urban reconstruction from point clouds," in *Computer Vision—ECCV 2016*. Cham, Switzerland: Springer, 2016, pp. 54–69.

[34] L. Nan and P. Wonka, "PolyFit: Polygonal surface reconstruction from point clouds," in *Proc. IEEE Int. Conf. Comput. Vis. (ICCV)*, Oct. 2017, pp. 2372–2380.

[35] X. Liu, Y. Zhang, X. Ling, Y. Wan, L. Liu, and Q. Li, "TopoLAP: Topology recovery for building reconstruction by deducing the relationships between linear and planar primitives," *Remote Sens.*, vol. 11, no. 11, p. 1372, Jun. 2019.

[36] J.-P. Bauchet and F. Lafarge, "Kinetic shape reconstruction," *ACM Trans. Graph.*, vol. 39, no. 5, pp. 1–14, Oct. 2020.

[37] L. Xie et al., "Combined rule-based and hypothesis-based method for building model reconstruction from photogrammetric point clouds," *Remote Sens.*, vol. 13, no. 6, p. 1107, Mar. 2021.

[38] M. Garland and P. Heckbert, "Surface simplification using quadric error metrics," in *Proc. 24th Annu. Conf. Comput. Graph. Interact. Techn.* Reading, MA, USA: Addison-Wesley, 1997, pp. 209–216.

[39] D. Cohen-Steiner, P. Alliez, and M. Desbrun, "Variational shape approximation," in *Proc. ACM SIGGRAPH Papers*, Aug. 2004, pp. 905–914.

[40] D. Salinas, F. Lafarge, and P. Alliez, "Structure-aware mesh decimation," *Comput. Graph. Forum*, vol. 34, no. 6, pp. 211–227, Sep. 2015.

[41] Z. S. GharehTappeh and Q. Peng, "Simplification and unfolding of 3D mesh models: Review and evaluation of existing tools," *Proc. CIRP*, vol. 100, pp. 121–126, Jan. 2021.

[42] M. Li and L. Nan, "Feature-preserving 3D mesh simplification for urban buildings," *ISPRS J. Photogramm. Remote Sens.*, vol. 173, pp. 135–150, Mar. 2021.

[43] T. Kelly, J. Femiani, P. Wonka, and N. J. Mitra, "BigSUR: Large-scale structured urban reconstruction," *ACM Trans. Graph.*, vol. 36, no. 6, pp. 1–16, Dec. 2017.

[44] Y. Verdie, F. Lafarge, and P. Alliez, "Lod generation for urban scenes," *ACM Trans. Graph.*, vol. 34, no. 3, p. 30, 2015.

[45] V. Bouzas, H. Ledoux, and L. Nan, "Structure-aware building mesh polygonization," *ISPRS J. Photogramm. Remote Sens.*, vol. 167, pp. 432–442, Sep. 2020.

[46] Y. Tian, M. Gerke, G. Vosselman, and Q. Zhu, "Knowledge-based building reconstruction from terrestrial video sequences," *ISPRS J. Photogramm. Remote Sens.*, vol. 65, no. 4, pp. 395–408, Jul. 2010.

[47] E. Kwak and A. Habib, "Automatic representation and reconstruction of DBM from LiDAR data using recursive minimum bounding rectangle," *ISPRS J. Photogramm. Remote Sens.*, vol. 93, pp. 171–191, Jul. 2014.

[48] H. Fan, W. Yao, and Q. Fu, "Segmentation of sloped roofs from airborne LiDAR point clouds using ridge-based hierarchical decomposition," *Remote Sens.*, vol. 6, no. 4, pp. 3284–3301, Apr. 2014.

[49] Y. Zheng, Q. Weng, and Y. Zheng, "A hybrid approach for three-dimensional building reconstruction in Indianapolis from LiDAR data," *Remote Sens.*, vol. 9, no. 4, p. 310, Mar. 2017.

[50] K. Wu, W. Shi, and W. Ahmed, "Structural elements detection and reconstruction (SEDR): A hybrid approach for modeling complex indoor structures," *ISPRS Int. J. Geo-Inf.*, vol. 9, no. 12, p. 760, Dec. 2020.

[51] F. Lafarge and C. Mallet, "Creating large-scale city models from 3D-point clouds: A robust approach with hybrid representation," *Int. J. Comput. Vis.*, vol. 99, no. 1, pp. 69–85, Aug. 2012.

[52] J. Song, S. Xia, J. Wang, and D. Chen, "Curved buildings reconstruction from airborne LiDAR data by matching and deforming geometric primitives," *IEEE Trans. Geosci. Remote Sens.*, vol. 59, no. 2, pp. 1660–1674, Feb. 2021.

[53] H. Fang, C. Pan, and H. Huang, "Structure-aware indoor scene reconstruction via two levels of abstraction," *ISPRS J. Photogramm. Remote Sens.*, vol. 178, pp. 155–170, Aug. 2021.

[54] W. Zhang, Z. Li, and J. Shan, "Optimal model fitting for building reconstruction from point clouds," *IEEE J. Sel. Topics Appl. Earth Observ. Remote Sens.*, vol. 14, pp. 9636–9650, 2021.

[55] M. Satari, F. Samadzadegan, A. Azizi, and H.-G. Maas, "A multi-resolution hybrid approach for building model reconstruction from LiDAR data," *Photogramm. Rec.*, vol. 27, no. 139, pp. 330–359, Sep. 2012.

[56] R. Tarjan, "Depth-first search and linear graph algorithms," *SIAM J. Comput.*, vol. 1, no. 2, pp. 146–160, Jun. 1972.

[57] *Boost C++ Libraries*. [Online]. Available: https://www.boost.org/

[58] *The Computational Geometry Algorithms Library*. [Online]. Available: https://www.cgal.org/
[59] L. Nan, "Easy3D: A lightweight, easy-to-use, and efficient C++ library for processing and rendering 3D data," *J. Open Source Softw.*, vol. 6, no. 64, p. 3255, Aug. 2021.
[60] M. Li, L. Nan, and S. Liu, "Fitting boxes to Manhattan scenes using linear integer programming," *Int. J. Digit. Earth*, vol. 9, no. 8, pp. 806–817, Aug. 2016.
[61] M. Guthe, P. Borodin, and R. Klein, "Fast and accurate Hausdorff distance calculation between meshes," *J. WSCG*, vol. 13, no. 2, pp. 41–48, 2005.

Li Yan (Member, IEEE) received the B.S., M.S., and Ph.D. degrees in photogrammetry and remote sensing from Wuhan University, Wuhan, China, in 1989, 1992, and 1999, respectively.

He is currently a Luojia Distinguished Professor with the School of Geodesy and Geomatics, Wuhan University. His research interests include photogrammetry, remote sensing, and precise image measurement.

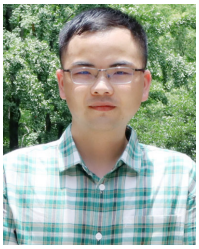

Yao Li received the M.S. degree in photogrammetry and remote sensing from Wuhan University, Wuhan, China, in 2018, where he is currently pursuing the Ph.D. degree under the supervision of Prof. Li Yan.

His research interests include photogrammetry and autonomous mobile measurement.

Jicheng Dai received the M.S. degree in photogrammetry and remote sensing from Wuhan University, Wuhan, China, in 2019, where he is currently pursuing the Ph.D. degree under the supervision of Prof. Li Yan.

His research interests include light detection and ranging (LiDAR) SLAM and multisensor fusion.

Hong Xie received the B.S., M.S., and Ph.D. degrees in photogrammetry and remote sensing from Wuhan University, Wuhan, China, in 2007, 2009, and 2013, respectively.

He is currently an Associate Professor with the School of Geodesy and Geomatics, Wuhan University. His research interests include mobile 3-D laser scanning technology, computer vision, and autonomous mobile measurement robots.